CELLULAR PATHWAYS AFFECTED BY CARBON NANOPOWDER-BENZO(α)PYRENE COMPLEX IN HUMAN SKIN FIBROBLASTS IDENTIFIED BY PROTEOMICS

Binelli[a*] A., S. Magni[a*], C. La Porta[bf], L. Bini[c], C. Della Torre[a], M. Ascagni[ad], D. Maggioni[e], A. Ghilardi[a], A. Armini[c], C. Landi[c], N. Santo[ad], L. Madaschi[ad], V. Coccè[g], F. Mutti[bf], M.C. Lionetti[bf], E. Ciusani[h], L. Del Giacco[a]

[a]Department of Biosciences, University of Milan, Italy; [b]Department of Environmental Science and Policy, University of Milan; [c]Department of Life Science, University of Siena, Italy; [d]UNITECH-NOLIMITS platform, University of Milan; [e]Department of Chemistry, University of Milan; [f]Center for Complexity & Biosystem, University of Milan, [g]Department of Biomedical, Surgical and Dental Sciences, University of Milan, [h]Department of Diagnostics and Applied Technology, Istituto Neurologico Carlo Besta, Milan.

Abstract

One of the crucial and unsolved problems of the airborne carbon nanoparticles is the role played by the adsorbed environmental pollutants on their toxicological effect. Indeed, in the urban areas, the carbon nanoparticles usually adsorb some atmospheric contaminants, whose one of the leading representatives is the benzo(α)pyrene. Herein, we used the proteomics to investigate the alteration of toxicological pathways due to the carbon nanopowder-benzo(α)pyrene complex in comparison with the two contaminants administered alone on human skin-derived fibroblasts (hSDFs) exposed for 8 days in semi-static conditions. The preliminary confocal microscopy observations highlighted that carbon-nanopowder was able to pass through the cell membranes and accumulate into the cytoplasm both when administered alone and with the adsorbed benzo(α)pyrene. Proteomics revealed that the effect of carbon nanopowder-benzo(α)pyrene complex seems to be related to a new toxicological behavior instead of simple additive or synergistic effects. In detail, the cellular pathways modulated by the complex were mainly related to energy shift (glycolysis and pentose phosphate pathway), apoptosis, stress response and cellular trafficking.

Keywords: Nanoparticles, Hydrocarbons, Particulate matter, Omics.

* Corresponding Authors: Andrea Binelli (andrea.binelli@unimi.it); Stefano Magni (stefano.magni@unimi.it), Department of Biosciences, University of Milan, Via Celoria 26, 20133 Milan (Italy)

Introduction

One of the most important atmospheric pollutants are the airborne nanosized particles (NSPs; <100 nm) which affect the human health mainly in the urban areas. Among the NSPs, the carbon nanoparticles (CNPs) occupy a special place as priority pollutants since they are the main component of particulate matter with dimensions lower than 10 μm (PM_{10}) and 2.5 μm ($PM_{2.5}$). CNPs are composed by several natural and engineered classes, including fullerenes, nanotubes, carbon-black and black carbon. The CNPs can be naturally produced as weathering products from graphitic carbon in rocks (Dickens et al. 2004), but also as by-product of incomplete combustion of fossil fuel and vegetation (Cochrane, 2003). The rapid development of nanotechnologies and CNPs' production leads on one side to an increase of exposure, and on the other hand to the understanding of their effects on the health of animals and humans. In the last decade, several studies showed the capability of the CNPs to enter the organism through the respiratory and digestive systems, but also through the skin, in particular for the CNPs with lower dimension (Teow et al., 2011). The main effects whose CNPs are responsible are due to the overproduction of reactive oxygen species (ROS; Souza et al., 2017) that secondarily can induce genotoxicity (Totsuka et al., 2009). Furthermore, ROS induced by nanoparticles has shown to be also involved in asthma, lung cancer, pulmonary fibrosis and systemic cardiovascular disorders (Donaldson et al., 2005). On the other hand, it has been suggested that the toxicity of nanomaterials could be increased by some environmental contaminants adsorbed at the surface (Nowack et al., 2007) through a Trojan horse mechanism (Limbach et al., 2007). Because of their sources, methods of production and their large surface areas, commercial carbon blacks typically contain varying quantities of adsorbed by-products, such as aromatic compounds, derived from the production process (IARC, 2010). In particular, PAHs (polycyclic aromatic hydrocarbons) account about for 39-75% of organic impurities extractable with solvents from CNPs (Watson et al., 2001), whose B(α)P is one of the main component heavily released in urban areas and one of the environmental contaminants more dangerous, so that it is listed as a Group 1 (carcinogenic for humans) by IARC (2010).

Since there are few studies investigating the interactions of CNPs and volatile contaminants, herein we investigated the possible effect of the interaction between a particular carbon black-like powder, the carbon nanopowder (CNPW), and benzo(α)pyrene (B(α)P) on the whole proteome profile in human skin fibroblasts (hSDFs). These cells are very useful for this kind of studies, considering that the skin is one of the major target of these atmospheric pollutants, as suggested by Drakaki and collaborators (2014 and citation therein) who showed that oxidative stress caused by PM was related to the extrinsic skin aging, while PAHs could induce skin cancer and acneiform eruptions. In addition, the hSDFs used in this study are non-transformed primary cell line, allowing to highlight the eventual effects of selected contaminants on natural physiological processes, while transformed

cells might change the physiological effect of nanoparticles, such as exposure time and concentration.

To investigate the toxicity of the CNPW-B(α)P complex and to elucidate the mechanism of action (MoA), we exposed the hSDF to CNPW and B(α)P alone and in co-exposure for 8 days. We applied the high-throughput methodology of proteomics to investigate the effects made by the single contaminants and the CNPW-B(α)P complex because it enables the understanding the structure, function and interactions of the whole protein content of cells. The use of a simple freeware allowed to demonstrate how proteins assemble in larger complexes, identifying common pathways involved in the pollutants' action. Contemporarily, we applied some advanced microscopy techniques to characterize the CNPW and to check its intake in the hSDFs, fortifying the information made by proteomics.

Materials and methods

The novelty of our approach lies in the way to administer the two contaminants when in co-exposure. Generally, the two pollutants are administered separated to the selected biological model, making three different components: the two fractions related to the single pollutants and the fraction composed by the complex of them. This generate an interfering situation that makes impossible to distinguish the actual effect exerted by the complex from the ones due to the single contaminants freely dissolved in the medium. In order to solve this confusing aspect, we preliminarily cleaned up the CNPW, eliminating any possible interfering organic chemicals, then we doped the cleaned CNPW with the appropriate concentration of B(α)P. This approach allowed the administration of the CNPW-B(α)P complex to the hSDFs without the confounding presence of the single pollutants.

Materials

CNPW (CAS no. 7440-44-0) and all solvents used (pesticide grade) were from Sigma-Aldrich (Steinheim, Germany), while B(α)P and PAH (PAH-Mix 14) standards were purchased by Dr. Ehrenstorfer (Augsburg, Germany). CNPW was characterized by high trace metal purity (≥99%) and a particle size <50 nm.

CNPW clean-up and B(α)P contamination

CNPW was preliminary cleaned-up with toluene by consecutive washes in a Soxhlet (FALC, Treviglio, Italy) for 92 h. We followed the decreasing trend of the large quantity of PAHs adsorbed on the CNPW particles by the collection of extracts at different times (24, 48, 58 and 92 h) and the following analysis by mass spectroscopy (GC-MS/MS). The cleaned CNPW was dried by Rotavapor and nitrogen flux, and stored in dark glass bottles. The dried CNPW was separated in

two glass bottles (500 mL) containing MilliQ® water, maintaining these suspensions in stirring for 48 h, which were previously sonicated by a probe sonicator (Stimin s.a.s, Giussano, Italy) for 15 min at 12 kHz. The first one was doped with 1 mg/L B(α)P, while the second was not contaminated. The two suspensions were then stirred for 48 h in the dark and centrifuged at 3000 x g for 30 min. The supernatants were stored at 4 °C for the check of the possible presence of B(α)P, while the precipitated CNPW was dried for 3-4 days in a muffle furnace. The quantity of B(α)P really adsorbed on CNPW was measured by a gas-chromatographer (GC-MS/MS, Trace GC Ultra, Thermo Finnigan, CA, USA) equipped with a mass spectrometer (Polaris Q, Thermo Finnigan) following the same analytical procedure described above. Lastly, we also measured the amount of B(α)P dissolved in the supernatants by a liquid/liquid extraction and GC-MS/MS.

CNPW characterization

The DLS (dynamic light scattering; Zetasizer Nano, Malvern, UK) was used to determine the hydrodynamic diameters and surface changes (ζ potentials) of CNPW. The instrument was equipped with a solid-state He-Ne laser operating at a wavelength of 633 nm and detecting the scattered light at a scattering angle of 173°. Each measurement was recorded in quadruplicate. Data were elaborated using Zetasizer Nano Series software, version 7.02 (Particular Sciences, UK). We determined the primary particle diameter and shape of CNPW by TEM and SEM (scanning electron microscopy). The SEM (Zeiss LEO 1430) coupled with a Centaurus detector for energy-dispersive X-ray (EDX) spectroscopy were used to analyze the morphology and purity of the bulk form of CNPW. The powder was mounted onto an aluminum SEM stub and gold-coated. Elemental analysis was performed using Oxford Instruments INCA ver. 4.04 software (Abingdon, UK). Morphology and size distribution of the CNPW were measured by TEM: purified CNPW was suspended in distilled water, stirred and then sonicated. Aliquots of 5 mL were deposited onto Formvar-coated, 300 mesh, copper grids, and the excess water was gently blotted using filter paper. Once dried, the grids were directly inserted into a Zeiss LEO 912 ab Energy Filtering transmission electron microscope operating at 120 kV, and images were collected at a magnification of 25,000 using a CCD-BM/1K system.

Cell culture and treatments

Human primary dermal fibroblasts (hSDF) (HuDe/BSPRC41) was provided from Centro Substrati Cellulari, ISZLER (Brescia, Italy) and cultured in EMEM (Euroclone, Milan, Italy) containing 1% L-Glutamine, 1% Penicillin/Streptomycin and 10% FBS (basal medium) at 37 °C in 5% CO_2 for no more than 10 passages. Sub-confluent cells were then incubated for 8 days in semi-static conditions with:

1. basal medium (control)

2. vehicle (dimethyl sulfoxide; DMSO 0.1%)
3. CNPW 50 mg/L
4. B(α)P 20 μg/L (dissolved in DMSO)
5. CNPW 50 mg/L+B(α)P 20 μg/L

The medium containing pollutants, vehicle or basal medium has been changed every day with the same fresh medium, adding the related quantity of contaminants. Results of CNPW and CNPW-B(α)P complex were compared with those of the control on the complete medium, while B(α)P results were compared with those of its carrier (DMSO). Three different flasks with Eagle's minimal essential medium were set up for each experimental group, to which FBS 10% (fetal bovine serum), penicillamine-streptomycin 1% and L-glutamine were added. About 1.5 millions of hSDFs were plated on each flask in triplicates, for a total of 4,5 millions cells for every experimental group. The medium was eliminated at the end of experiments and the flasks were washed with 5 mL of phosphate buffered saline (PBS) buffer 1x. Fibroblasts were detached from the flasks by the addition of trypsin (3 mL) and then incubated for 5 min. Lastly, 4 mL of medium were re-added to the samples that were then transferred into 15 mL tubes. Samples were centrifuged for 5 min at 800 rpm and the pellets were recovered in 2 mL of PBS 1x. Lastly, they were put on cryovials and centrifuged again for 5 min at 1,500 rpm. The supernatants were discarded and the fibroblasts were frozen in liquid nitrogen in 1.5 mL tubes. For the confocal observations, the hSDFs were stained for mitochondria using 400 nM MitoTracker Red CMXRos (Invitrogen, USA, cod. MP 7512) in growth medium for 45 min at 37 °C. Then, cells were washed twice with PBS (phosphate buffered saline) and replaced with basal medium. Z-stacks of hSDFs were acquired by Leica SP2 laser scanning confocal, using the reflection mode for the visualization of nanoparticle aggregates.

Cell Cycle Analysis and flow cytometry

Sub-confluent hSDFs were harvested by trypsinization, pelleted and fixed in 70% cold ethanol and subsequently stained with propidium iodide (PI, cod. P4864, Sigma) for 30 minutes at 4 °C. PI fluorescence was analyzed using FACS Vantage SE Becton Dickinson flow cytometry. The percentages of hSDFs in each phase of the cell cycle were calculated using FlowJO, LLC software. The hSDF are exposed to increasing concentration of nanoparticles (range 10-100 μg/mL) for 8 days, harvested and immediately analyzed by flow cytometry for the evaluation of forward scatter (FSC) and side scatter (SSC).

Proteomics analysis

The protocol of the fibroblast preparation for the following proteomics analysis consisted firstly in the hSDFs homogenization by a pestle in 400 μL of ice-cold buffer (Tris-HCl pH 7.5; EDTA;

EGTA; fenilmetilsulfonilfluoride in ethanol; protease inhibitor cocktail; Triton X-100) and the subsequent centrifugation at 13,000 rpm for 10 min at 4 °C. The proteins contained in the supernatant were quantified by the BCA (bicinchoninic acid) method in spectrophotometry (λ=562 nm) using the BSA (bovine serum albumin) as standard. The glycerol was then added to the homogenate which was frozen to -80 °C. 150 μg of proteins for each sample were precipitated using a chloroform/methanol/water mixture (4:1:3 v/v) and resolubilized in an adequate buffer. The first dimension (1-DE) was achieved using 18 cm of pH 3–10 non-linear gradient IPG strips (GE Healthcare, Milan, Italy) and an Ettan IPGphor II system (GE Healthcare, USA). The strips were then loaded onto a 12% acrylamide gel (24 cm length, 1 mm thickness) and run in an Ettan DALTsix electrophoresis unit (GE Healthcare). The gels were dyed with silver stain (ProteoSilver Plus Silver Stain Kit; Sigma Aldrich). Gel images were acquired by an ImageScanner II and analysed by ImageMaster 2D Platinum software (Amersham Biosciences, USA). The spots were statistically ($p<0.05$) evaluated in terms of the mean relative volume. A minimum 2-fold change cut-off relative to the controls was also employed. The proteins were firstly identified by MALDI-TOF/TOF (matrix-assisted laser desorption/ionization-time of flight/time of flight) mass spectrometry (Bruker Daltonics, Billerica, MA, USA), followed by the LC-ESI/MS-MS (Liquid chromatography electrospray ionization-tandem MS) Micro-HPLC Pump Phoenix 40 (Thermo Finnigan, San Jose, CA, USA) equipped with the LCQ DECA IT mass spectrometry (Thermo Finnigan) to confirm the identification. Spectra were analyzed by the *Turbo*SEQUEST algorithm (Thermo Finnigan). Using the online MASCOT MS/MS ion search software, MS/MS database searching was carried out in the NCBI nr or Swiss-ProtKB databases. Only peptides with individual ion scores of less than 0.05 ($p<0.05$) were considered significant.

Results

CNPW clean-up

CNPW was bought as a commercial standard, however the preliminary clean-up revealed a high contamination due to PAHs. In detail, the low-condensed (3-4 rings) PAHs, such as phenanthrene, 2-methilnaftalene and pyrene, highlighted a greater contamination of the CNPW in comparison with the high-condensed ones (5-6 rings), but also a higher capacity to be cleaned just after 24 h. On the contrary, the most hydrophobic PAHs needed a longer clean-up until 92 h. This is due to the van der Waals forces which are greater among the CNPW and molecules with a high steric hindrance (Powers et al., 2006). Anyway, the selected procedure to eliminate the PAHs adsorbed on the CNPW was extremely efficient since the total PAH concentration decreased from 14 ppm (0.0014% of the total carbon mass) to 0.03 ppm (0.00003% of the total carbon mass).

CNPW characterization

This step was crucial since some physical characteristics, such as dimension, charge and state of aggregation, might interfere with the interactions with the biological structures (Powers et al., 2006). The ξ potential (-30.9±3.05 mV) analyses highlighted a negative surface charge of the bulk CNPW, according to Hussein and co-workers (2009), and a mean hydrodynamic diameter of 822 nm (by DLS). These data indicated a clear aggregation behavior of CNPW particles despite the negative ξ potential value, while the hydrodynamic range was much higher than 100 nm, upper limit that usually defines the nanoparticles. Actually, SEM and TEM images showed the presence of two separated fractions in the CNPW composition (Fig. 1): one fraction was formed by many graphite-like sheets closely attached to one another (Fig. 1A) and the second was composed by nanometric particles of approximately 20 nm in size (Fig. 1B).

Selection of concentrations

Preliminary range-findings were needed to select both CNPW and B(α)P concentrations avoiding any possible acute effect on hSDFs. We used two complementary strategies for the selection of CNPW concentration: first of all, we verified if this kind of contaminant was able to affect the proliferative capability of hSDFs through a cell cycle analysis. As shown in Fig. 2A, a CNPW concentration higher than 50 mg/L altered significantly ($p<0.05$) the proliferative capability of cells. Furthermore, we carried out flow cytometry experiments of hSDFs exposed for 8 days to increasing concentrations of CNPW (Fig. 2B, C). As far as the CNPW concentration raised, we observed a clear increase of cell volume, measured as side scatter (SSC), reaching a plateau at 100 mg/L. Thus, combining these results, we selected 50 mg/L of CNPW as the concentration to be administered in the definitive exposures. In the case of B(α)P, we selected the concentration based on the B(α)P really adsorbed on the 50 mg/L CNPW during the preliminary tests (Della Torre et al., 2017). Since we measured 344.6 μg B(α)P/g CNPW, for a total of about 17 μg B(α)P sorbed on 50 mg of CNPW, we set to 20 μg/L the B(α)P concentration corresponding to suspensions containing 50 mg/L of CNPW. Moreover, this B(α)P concentration did not induce any kind of acute effect on hSDFs (data not shown). An in-depth explanation of the preliminary tests conducted for the doses selection is shown in our previous paper (Della Torre et al., 2017).

Confocal microscopy observations

The z-stack maximum projections showed the presence of CNPW particles in the hSDFs already after 24 h of exposure both after CNPW (Fig. 3B) and CNPW-B(α)P complex (Fig. 3C) exposures. This means that CNPW is able to pass through the biological barriers and accumulate in the cytoplasm without killing the cell, as also demonstrated by the presence of many CNPW aggregates

present in a hSDF (Fig. 3C). The same behavior was shown after 8 days of exposure (Fig. 3E, F) when fibroblasts reached the confluence status.

Proteomics

The spots shown in the gels (n=4) were compared with the related controls (n=4): B(α)P administered alone *vs* solvent control (DMSO), while the CNPW administered alone and CNPW-B(α)P complex *vs* control from the growth medium for cell culture. We found in each gel about 1,000 different spots, of which 240 were shared between solvent control and B(α)P, 410 between the growth medium control and CNPW, and lastly 292 between the growth medium control and CNPW-B(α)P complex. We only took into account spots with a significant difference (Student t-test, *p<0,05, **p<0,01) in terms of volume percentage: 23 spots for the experiment with B(α)P, 31 spots for CNPW 50 mg/L and 71 spots for CNPW 50 mg/L+B(α)P 20 μg/L. To be more protective, we considered another cut-off based on the variation in terms of volume percentage between comparable spots higher than 2 times at least (fold change % volume/volume). Thus, we evaluated a modulation of 7 proteins after the exposure to B(α)P with an up-regulation for only one of them, while the other proteins exhibited a significant ($p<0.05$) down-regulation (Fig. 4A). The following analysis step identified only two proteins (corresponding to spots n. 6 and 9), while the identification of the remaining other five was not possible because of the scarce material recovered by the spots. The exposure to CNPW administered alone caused an up-regulation of 7 proteins and a down-regulation of 2 of them (Fig. 4B). Once again, the few quantity of material in each spot allowed the identification of only 3 proteins, corresponding to spots n. 4, 18 and 31. The exposure to CNPW-B(α)P complex modulated 47 different proteins: 21 of them were up-regulated and 26 down-regulated (Fig. 4C). Thirty proteins were identified. In the additional tables S1, S2 and S3 are shown the complete characteristics of the identified proteins.

Discussion

The aim of this study was the evaluation of protein amount change in primary cultures of hSDFs exposed to CNPW or B(α)P alone and in co-exposure (CNPW-B(α)P complex) to identify both the MoA and the role played by CNPW as possible carrier towards B(α)P and its relationship with the toxicity. Proteomics showed that CNPW-B(α)P complex (Fig. 4C) induced a higher number of proteins differentially regulated with respect to single treatments (Figs. 4A, B), suggesting a possible effect of CNPW in facilitating the intake of B(α)P, as also observed by the confocal microscopy (Fig. 3F). Moreover, we observed that the complex altered significantly also the toxic potency of single pollutants. Indeed, we did not identify any changed proteins in common among the three treatments, showing not only that the chemical and physical pollutant possess different

MoA, as expected, but especially that the two contaminants bound together achieved a different toxic behavior against diverse cellular targets, as in-depth explained below.

B(α)P probably acted as inhibiting agent on the cell metabolism since it was able to down-regulate 6 different proteins out of the 7 modulated (Fig. 4A). In detail, we identified the same protein (*Heat shock cognate 71 kDa protein*, HSPA8) in the spot 6 and 9 (Fig. 4A) as a consequence of post-translational modifications. HSPA8 is part of the big Heat Shock Protein 70 (HSP70) family, which is highly conserved in different sub-cellular compartments, such as cytoplasm, nucleus, endoplasmic reticulum and mitochondria (Robert et al., 2003). Their production is increased not only to make a homeostatic response to high temperatures, but in general as response to stress conditions, such as UV ray (Cao et al., 1999), low temperature exposure (Matz et al., 1995) and during the tissue damage recovery (Laplante et al., 1998). Moreover, Li and co-workers (2000) proved the role of HSP70 in preventing the activation of caspase-3 in human macrophages and the consequent inhibition of apoptosis. More in detail, the down-regulation of some proteins of this family, included the HSPA8, increased the sensitivity against many apoptotic agents (Jäättelä et al., 1998). In our experiments, the down-regulation of HSPA8 due to B(α)P exposure is congruent with its well-known genotoxicity and confirms other studies in which an increase of caspase-3 activity was observed in hematopoietic stem cells (Van Grevenynghe et al., 2005) and DNA laddering in cells derived from human carcinoma (Park et al., 2006) after B(α)P administration.

A different proteins' modulation behavior was notice after CNPW exposure since cells seemed to increase the protective pathways by the up-regulation of 7 proteins out of the 9 changed (Fig. 4B). Although we identified only 3 proteins, it is very interesting that 2 of them (*Vimentin* and *Heat shock protein beta-1*) are related to cytoskeleton architecture, in agreement with previous observation made in zebrafish embryos (Binelli et al., 2017). This result appeared very interesting since it showed that CNPW can act in a similar manner along the biological scale. The only down-regulated protein identified was the HSPB1 (*Heat shock protein beta-1,* also known as HSP27) that interestingly belong to the same HSP70 family of the HSPB8 modulated by B(α)P. The HSPB1 is a chaperonin that plays a role in stress resistance and actin organization. Thus, its down-regulation after CNPW exposure can suggest a possible interference with cell organization, as well as to counteract thermal resistance. Another varied protein involved in the cytoskeleton organization was VIM (*Vimentin*) that is highly expressed in fibroblasts and whose main function is the fixing of cell organelles to cytoplasm (Sommers et al., 1989). The study carried out by Mou and co-workers (2010), in which the overregulation of VIM compromised the denucleation of crystalline fibers and the cataract onset, pointed out as the eye development can be one of the main targets of CNPW, as also highlighted in the above-mentioned study on zebrafish embryos (Binelli et al., 2017). The last identified protein was the UBA52 (Ubiquitin-60S ribosomal protein L40), a structural component of the 60 S ribosomal subunit. UBA52 is a ubiquitin highly conserved in all eukaryotes' tissues whose

317 main roles are related to protein degradation, maintaining of chromatin structure, gene expression
318 and stress response (Lee et al., 2013).
319 The higher number of proteins modulated showed the greater capacity of the CNPW-B(α)P
320 complex to interfere on different cellular pathways (Fig. 4C), magnifying the effect of the single
321 contaminants. We analyzed the entire data-set of these modulated proteins though the freeware
322 STRING (www.string-db.org) to identify the cellular pathways affected by the complex between
323 the two different contaminants. The main cellular networks modified by the CNPW-B(α)P complex
324 are the glycolysis and pentose phosphate pathway (PPP) since 12 proteins out of the 30 identified
325 are involved in these two metabolic pathways. Actually, several spots were identified as the same
326 protein, suggesting post-translational modification events, which allowed the identification of 7
327 different proteins involved in these pathways (Fig. 5A). Glycolysis and PPP are complex and strong
328 correlated pathways (Fig. 6) that produce mainly ATP (adenosine triphosphate) and NADPH
329 (nicotinamide adenine dinucleotide phosphate). Very interestingly, the CNPW-B(α)P complex
330 induced a general drop of glycolytic function due to the diffuse under-regulation of all the enzymes
331 (glyceraldehyde 3-phosphate dehydrogenase excluded; Fig. 6). By contrast, at least the first phase
332 of the PPP seemed not to be compromised because the enzymes down-regulated are located
333 downstream of the oxidative phase in which NADPH is generated (Fig. 6). The transketolase (TKT)
334 and partially the trans-aldolase (T-ALDO) are the key-regulators between the PPP and glycolysis
335 since they convert the ribose-5 phosphate produced in the first phase of PPP into glycolytic
336 intermediates (fructose-6 phosphate and glyceraldehyde-3 phosphate). Whereas the TKT was
337 significantly down-regulated after the co-exposure, the amount of some proteins necessary for the
338 correct completion of glycolysis decreased, bringing back about all the other enzymes involved in
339 the final phase of the pathway, namely the fructose-bisphosphate aldolase A (ALDOA),
340 triosephosphate isomerase 1 (TPI1), phosphoglycerate kinase 1 (PGK1), α-enolase (ENO-1) and
341 pyruvate kinase (PKM; Fig. 6). Furthermore, another key glycolytic enzyme is TPI1 which is able
342 to reroute the carbohydrate flux from glycolysis to PPP to counteract oxidative stress and the
343 consequent imbalance of redox state in cytoplasm (Ralser et al., 2007). In fact, PPP is one of the
344 main pathways to obtain NADPH that is required as redox cofactor by some antioxidant enzymes to
345 neutralize ROS (Pollak et al., 2007) and for the cytochrome P450 (CYP 450) to hydroxylate the
346 aromatic compounds, such as B(α)P. NADPH is reduced in the cytosol from $NADP^+$ by many
347 enzymes, 2 of them catalyzing the first phase of PPP (Fig. 6): the glucose 6-phosphate
348 dehydrogenase (G6PD) and 6-phosphogluconate dehydrogenase (PGD), whose activity was
349 actually not modified after the exposure to the CNPW-B(α)P complex. Apparently, the over-
350 regulation of the glyceraldehyde-3 dehydrogenase (GADPH; Fig. 6) seems to represent a
351 contradictory result. Actually, a study of Colussi and co-workers (2000) demonstrated that GADPH
352 is a target of a strong oxidant (H_2O_2) only when the glycolysis is active, suggesting that GADPH

inactivation is not the simple consequence of its arrest. They also showed that, in presence of two well-known glycolysis inhibitors (2-deoxyglucose or cytochalasin B), H_2O_2 was not able to inactivate GADPH, whose activity was instead slightly increased. Thus, our results seemed to suggest an inhibition of glycolysis and a consequent redirection of carbohydrate flux to PPP in order to keep up the production of NADPH to counteract the oxidative stress produced by the CNPW-B(α)P complex, which was also observed by Della Torre and co-workers (2017) in the teleosteous *Danio rerio* (zebrafish). The block of glycolysis can be also view as a protective response of cells to apoptosis induced by oxidant agents, highlighting that this cellular response can be a self-protecting action instead of a passive result of the oxidative injury (Colussi et al., 2000). Lastly, the increase of GADPH amount could be also due to the plethora of other metabolic processes in which this protein is involved, such as DNA repair, tRNA export, membrane fusion and transport, cytoskeletal dynamics and the above-mentioned cell death (Tristan et al., 2011).

The exposure to CNPW-B(α)P complex modulated other proteins involved in different biological pathways. In detail, we found 6 proteins implicated in the cytoskeleton formation and apoptotic mechanism (Fig. 5B): Profilin 1 (PFN1), Peptidyl-prolyl cis-trans isomerase A (PPIA), 60 kDa Heat shock protein (HSPD1), Pyruvate kinase (PKM), fructose-bisphosphate aldolase A (ALDOA) and Cofilin-1 (CFL1). Some of them are strictly correlated to the apoptosis (Cheng et al., 2016), demonstrating once again the genotoxic effect of these two environmental contaminants inserted in the group 1 (B(α)P) and 2B (CNPW) by IARC (2010). Apparently, the two biological pathways described above seem to play opposite roles because the block of glycolysis was referred to a protective mechanism against apoptosis, while this second pathway suggests an increase of the programmed cell death, which however it can be considered as a homeostatic response to prevent systemic damage. Interestingly, the down-regulation of CFL1 is also involved in the homeostatic response to hypoxia through the cytoskeleton adaptation and actin assemblage (Mendelsohn et al., 2009). More specifically, this protein is part of the first step of physiological response to hypoxia before the activation of the second deeper phase related to transcriptional responses due to HIF (hypoxia inducible factors) genes. Since *Cfl1* was down-regulated also in zebrafish embryos exposed to 50 mg/L CNPW (Binelli et al., 2017), we suggest that this protein could be a preferential target just of the CNPW instead of B(α)P.

Eleven proteins modulated by the CNPW-B(α)P complex were implicated in the response to generic cell stress (Fig. 5C), 7 of them (PKM, CFL1, PFN1, HSPB1, ALDOA, GAPDH, PPIA) were present in the first two pathways described above. It is interesting to point out that HSPB1 was the only varied protein (down-regulated) in common between CNPW and CNPW-B(α)P complex exposures, suggesting a possible comparable MoA on the same target due to CNPW instead of B(α)P. However, the functions related to the class of heat-shock proteins are enormous and the same effect on the HSPB1 regulation could be only accidental. A new changed protein in this

specific pathway was instead the Glutathione S-transferase P (GSTP1) that is involved in the detoxification enzyme system of phase II. The drop of the GSTP1 amount could reduce the cellular response against planar lipophilic chemicals and in general the detoxification capability. This is confirmed by the study of Almeida and co-workers (2012) in which the down-regulation of GSTP1 establishes a drop of detoxification efficiency, with the consequent accumulation of cytotoxic and carcinogenic agents in head and neck squamous cell carcinoma. The down-regulation of GSTP1 confirmed one of the main results obtained in the previous study of Della Torre and collaborators (2017) in which they found a significant ($p<0.05$) decrease of the GST activity in zebrafish embryos exposed to the CNPW-B(α)P complex. Another protein interested in the response to oxidative stress was PSME2 (Proteasome activator complex subunit 2) that is part of the cytoplasmic PA28αβ proteasome regulator, implicated in the degradation of oxidized proteins (Pickering et al., 2010). The down-regulation of PSME2 can be view both as a decreasing capability to respond to oxidative stress, but also as an indication of the direct inactivation of proteasomes caused by oxidation (Reinheckel et al., 1998), due to the CNPW-B(α)P complex.

Lastly, 6 proteins are related to a pathway involved in the vesicle transport control (Fig. 5D), even if most of them are already described in the previous pathways. The only two new proteins belonging to this pathway were NME1 (Nucleoside-diphosphate kinase A, also known as NDPKs) and ANXA2 (Annexin A2). The first one is a fundamental protein for the synthesis of nucleotide triphosphates and it is fascinating to observe how it is correlated to glycolysis by a complex cell signaling pathway. In fact, it was shown that NMEs acts in high energy phosphoryl transfer and signal communication in network with other nucleotide metabolizing enzymes, including the glycolytic ones (Dzeja and Terzic, 2003). NMEs are located in mitochondria, cytosol and nucleus, favoring the channeling of nucleotide triphosphates into protein synthesis and DNA replication complexes (Gerbitz et al., 1996). Several reports indicated that a NME deficiency produced a highly biased nucleoside triphosphate pool in cells and a mutated phenotype (Bernard et al., 2000), as well as a rise of genetic error frequency (Bebenek et al., 1992). NME1 can be also involved in the homeostatic response to hypoxia, like the above mentioned CFL1, since its down-regulation determines the increase of two angiogenic factors, namely the interleukin 8 (IL-8) and vascular endothelial growth factor (VEGF), and the consequent proliferation of blood vessels in stromal cells (Kai-Kai et al., 2013). The over-regulation of VEGF was also caused by the up-regulation of ANXA2 in endometrial cells in human adenomyosis (Zhou et al., 2012), suggesting once again the possible role of the CNPW-B(α)P complex in the creation of a hypoxic status. The co-exposure modulated other proteins which were not involved in any pathways previously described: APRT (adenine phospho-ribosyl-transferase), CLIC4 (chloride intracellular channel protein 4) and ARHGDIA (Rho GDP-dissociation inhibitor 1).

Although the concentrations of CNPW and B(α)P used in this study are higher than environmental ones, the modulation of proteins in human fibroblasts can highlight a potential risk for workers in several industry productions, such as aluminum, petroleum industries and settings where combustion processes are involved.

Conclusions

This study represents a step-forward in the controversial debate about the possible role played by carbon nanoparticles to be a carrier for the adsorbed environmental pollutants since we demonstrated that the CNPW-B(α)P complex is able to enter in the human fibroblasts, confirming the skin as intake route. Surely, the most intriguingly effect revealed in this study was that the higher number of modulated proteins due to CNPW-B(α)P complex seemed to be related to a new toxicological behavior instead of simple additive or synergistic effects. Although it was not surprising the lack of common modulated proteins after the single exposures due to the different nature of the two compounds, the shift of the toxicological behavior noticed with the CNPW-B(α)P complex suggested the achievement of new different properties that result in different cellular targets, such as the pathways related to energy shift (glycolysis and PPP), apoptosis, stress response and cellular trafficking. Therefore, this study carried out by a high-throughput technology added another selling point to the intrinsic environmental danger of CNPs, and suggests an in-depth investigation of the relationships with other atmospheric contaminants which can increase their toxicological potency.

Acknowledgements

This study was financially supported by the “Cariplo Foundation”; grant number 2013-0817.

References

Almeida LO, Goto,RN, Pestana, CR, Uyemura SA, Gutkind S, Curti C, Leopoldino AM 2012. SET overexpression decreases cell detoxification efficiency: ALDH2 and GSTP1 are downregulated, DDR is impaired and DNA damage accumulates. Febs J. 279: 4615-4628.

Bebenek K, Roberts JD, Kunkel TA 1992. The effects of dNTP pool imbalances on frameshift fidelity during DNA replication. J. Biol. Chem. 267: 3589-3596.

Bernard MA, Ray NB, Olcott MC, Hendricks SP, Mathews CK 2000. Metabolic functions of microbial nucleoside diphosphate kinases. J. Bioenerg. Biomembr. 32: 259-267.

Binelli A, Del Giacco L, Santo N, Bini L, Magni S, Parolini M, Madaschi L, Ghilardi A, Maggioni D, Ascagni M, Armini A, Prosperi L, Landi C, La Porta C, Della Torre C. 2017. Carbon

458 nanopowder acts as a Trojan-horse for benzo(a)pyrene in *Danio rerio* embryos.
459 Nanotoxicology 11: 371-381.
460 Cao Y, Ohwatari N, Matsumoto T, Kosaka M, Ohtsuru A, Yamashita, S 1999. TGF-beta1 mediates
461 70-kDa heat shock protein induction due to ultraviolet irradiation in human skin fibroblasts.
462 Pflugers Arch. 438: 239-244.
463 Cheng S, Luo M, Ding C, Peng C, Lv Z, Tong R, Xiao H, Xie H, Zhou L, Wu J, Zheng S 2016.
464 Downregulation of Peptidylprolyl isomerase A promotes cell death and enhances doxorubicin-
465 induced apoptosis in hepatocellular carcinoma. Gene 591: 236-244.
466 Cochrane MA 2003. Fire science for rainforests. Nature 421: 913-919.
467 Colussi C, Albertini MC, Coppola S, Rovidati S, Galli F, Ghibelli L 2000. H_2O_2-induced block of
468 glycolysis as an active ADP- ribosylation reaction protecting cells from apoptosis. Faseb J. 14:
469 2266-2276.
470 Della Torre C, Parolini M, Del Giacco L, Ghilardi A, Ascagni M, Santo N, Maggioni D, Magni S,
471 Madaschi L, Prosperi L, La Porta C, Binelli A 2017. Adsorption of B(α)P on Carbon
472 Nanopowder affects accumulation and toxicity on zebrafish (*Danio rerio*) embryos. Environ.-
473 Sci. Nano 4: 1132-1146.
474 Dickens AF, Gelinas Y, Masiello CA, Wakeham S, Hedges JI 2004. Reburial of fossil organic
475 carbon in marine sediments. Nature 427: 336-339.
476 Donaldson K, Tran L, Jimenez LA, Duffin R, Newby DE, Mills N, MacNee W, Stone V 2005.
477 Combustion-derived nanoparticles: a review of their toxicology following inhalation exposure.
478 Part. Fibre Toxicol. 2: 10.
479 Drakaki E, Dessinioti C, Antoniou CV 2014. Air pollution and the skin. Front. Environ. Sci. 2, 11.
480 Dzeja, P.P., Terzic, A., 2003. Phosphotransfer networks and cellular energetics. J. Exp. Biol. 206:
481 2039-2047.
482 Gerbitz K, Gempel K, Brdiczka D 1996. Mitochondria and diabetes. Genetic, biochemical, and
483 clinical implications of the cellular energy circuit. Diabetes 45: 113-126.
484 Hussain S, Boland S, Baeza-Squiban A, Hamel R, Thomassen LCJ, Martens JA, Billon-Galland
485 MA, Fleury-Feith J, Moisan F, Pairon J-C, Marano F 2009. Oxidative stress and
486 proinflammatory effects of carbon black and titanium dioxide nanoparticles: role of particle
487 surface area and internalized amount. Toxicology 260: 142-149.
488 IARC (International Agency for Research on Cancer) 2010. IARC Monographs on the Evaluation
489 of Carcinogenic Risks to Humans. Volume 92: Some Non-Heterocyclic Polycyclic Aromatic
490 Hydrocarbons and Some Related Exposures. Edited by IARC, Lyon (France) pp. 853.
491 Jäättelä M, Wissing D, Kokholm K, Kallunki T, Egeblad M 1998. Hsp70 exerts its anti-apoptotic
492 function downstream of caspase-3-like proteases. Embo J. 17: 6124-6134.

493 Kai-Kai C, Li-Bing L, Li-Ping J, Yu-Han M, Jun S, Ying W, Jie M, Ming-Qing L, Da-Jin L 2013.
494 NME1 suppression of endometrial stromal cells promotes angiogenesis in the endometriotic
495 milieu via stimulating the secretion of IL-8 and VEGF. Int. J. Clin. Exp. Pathol. 6: 2030-2038.
496 Laplante AF, Moulin V, Auger FA, Landry J, Li H, Morrow G, Tanguay RM, Germain L 1998.
497 Expression of heat shock proteins in mouse skin during wound healing. J. Histochem.
498 Cytochem. 46: 1291-1301.
499 Lee AS, Burdeinick-Kerr R, Whelan SP 2013. A ribosome-specialized translation initiation
500 pathway is required for cap-dependent translation of vesicular stomatitis virus mRNAs. Roc.
501 Natl. Acad. Sci. U. S. A. 110: 324-329.
502 Li CY, Lee JS, Ko YG, Kim JI, Seo JS 2000. Heat shock protein 70 inhibits apoptosis downstream
503 of cytochrome c release and upstream of caspase-3 activation. J. Biol. Chem. 275: 25665-
504 25671.
505 Limbach LK, Wick P, Manser P, Grass RN, Bruinink A, Stark WJ 2007. Exposure of engineered
506 nanoparticles to human lung epithelial cells: influence of chemical composition and catalytic
507 activity on oxidative stress. Environ. Sci. Technol. 41: 4158-4163.
508 Matz JM, Blake MJ, Tatelman HM, Lavoi KP, Holbrook NJ 1995. Characterization and regulation
509 of cold-induced heat shock protein expression in mouse brown adipose tissue. Am. J. Physiol.
510 269: R38-47.
511 Mendelsohn BA, Malone JP, Townsend RR, Gitlin JD 2009. Proteomic analysis of anoxia tolerance
512 in the developing zebrafish embryo. Comp. Biochem. Physiol. D-Genomics Proteomics 4: 21-
513 31.
514 Mou L, Xu JY, Li W, Lei X, Wu Y, Xu G, Kong X, Xu GT 2010. Identification of vimentin as a
515 novel target of HSF4 in lens development and cataract by proteomic analysis. Invest.
516 Ophthalmol. Vis. Sci. 51: 396-404.
517 Nowack B, Bucheli TD 2007. Occurrence, behavior and effects of nanoparticles in the environment.
518 Environ. Pollut. 150: 5-22.
519 Park SY, Lee SM, Ye SK, Yoon SH, Chung MH, Choi J 2006. Benzo[a]pyrene-induced DNA
520 damage and p53 modulation in human hepatoma HepG2 cells for the identification of potential
521 biomarkers for PAH monitoring and risk assessment. Toxicol. Lett. 167: 27-33.
522 Pickering AM, Koop AL, Teoh CY, Ermak G, Grune T, Davies KJ 2010. The immunoproteasome,
523 the 20S proteasome and the PA28αβ proteasome regulator are oxidative-stress-adaptive
524 proteolytic complexes. Biochem. J. 432: 585-594.
525 Pollak N, Dolle C, Ziegler M 2007. The power to reduce: pyridine nucleotides - small molecules
526 with a multitude of functions. Biochem. J. 402: 205-218.

527 Powers KW, Brown SC, Krishna VB, Wasdo SC, Moudgil BM, Roberts SM 2006. Research
528 strategies for safety evaluation of nanomaterials. Part VI. Characterization of nanoscale
529 particles for toxicological evaluation. Toxicol. Sci. 90: 296-303.
530 Ralser M, Wamelink MM, Kowald A, Gerisch B, Heeren G, Struys EA, Klipp E, Jakobs C,
531 Breitenbach M, Lehrach H, Krobitsch S 2007. Dynamic rerouting of the carbohydrate flux is
532 key to counteracting oxidative stress. J. Biol. 6: 10.
533 Reinheckel T, Sitte N, Ullrich O, Kuckelkorn U, Davies KJ, Grune T 1998. Comparative resistance
534 of the 20S and 26S proteasome to oxidative stress. Biochem. J. 335: 637-642.
535 Robert J 2003. Evolution of heat shock protein and immunity. Dev. Comp. Immunol. 27: 449-464.
536 Sommers CL, Walker-Jones D, Heckford SE, Worland P, Valverius E, Clark R, McCormick F,
537 Stampfer M, Abularach S, Gelmann EP 1989. Vimentin rather than keratin expression in some
538 hormone-independent breast cancer cell lines and in oncogene-transformed mammary epithelial
539 cells. Cancer Res. 49: 4258-4263.
540 Souza JP, Baretta JF, Santos F, Paino IMM, Zucolotto V 2017. Toxicological effects of graphene
541 oxide on adult zebrafish (*Danio rerio*). Aquatic. Toxicol. 186: 11-18.
542 Teow Y, Asharani PV, Hande MP, Valiyaveettil S 2011. Health impact and safety of engineered
543 nanomaterials. Chem. Commun. 47: 7025-7038.
544 Totsuka, Y., Higuchi, T., Imai, T., Nishikawa, A., Nohmi, T., Kato, T., Masuda, S., Kinae, N.,
545 Hiyoshi K, Ogo S, Kawanishi M, Yagi T, Ichinose T, Fukumori N, Watanabe M, Sugimura T,
546 Wakabayashi K 2009. Genotoxicity of nano/microparticles in *in vitro* micronuclei, *in vivo*
547 comet and mutation assay systems. Part. Fibre Toxicol. 6: 1-11.
548 Tristan C, Shahani N, Sedlak TW, Sawa A 2011. The diverse functions of GADPH: views from
549 different subcellular compartments. Cell. Signal. 23: 317-323.
550 Van Grevenynghe J, Bernard M, Langouet S, Le Berre C, Fest T, Fardel O 2005. Human CD34-
551 positive hematopoietic stem cells constitute targets for carcinogenic polycyclic aromatic
552 hydrocarbons. J. Pharmacol. Exp. Ther. 314: 693-702.
553 Watson AY, Valberg PA 2001. Carbon black and soot: two different substances. Am. Ind. Hyg.
554 Assoc. J. 62: 218-228.
555 Zhou S, Yi T, Liu R, Bian C, Qi X, He X, Wang K, Li J, Zhao X, Huang C, Wei Y 2012.
556 Proteomics identification of annexin A2 as a key mediator in the metastasis and
557 proangiogenesis of endometrial cells in human adenomyosis. Mol. Cell. Proteomics 11:
558 M112.017988.

HIGHLIGHTS:

- Skin represents an alternative route of exposure for carbon nanoparticles.
- Carbon nanoparticles act as carrier for benzo(α)pyrene.
- Proteomics is a useful tool for the eco-nanotoxicological studies.

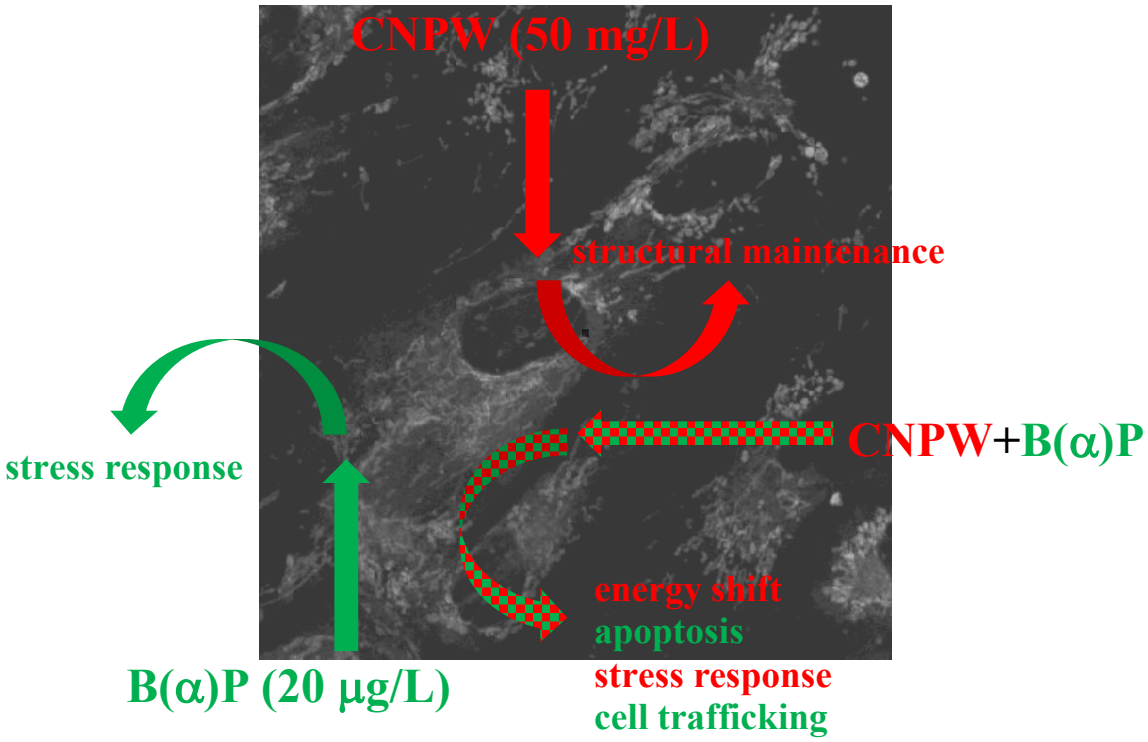

nanotoxicology quantifies at what extent each of these properties may pose a threat to the environment and human health

CAPTIONS

Figure 1 The two different fractions of CNPW visualized by SEM and TEM. A) graphite-like sheets observed by SEM; B) nanometric particulate component observed by TEM.

Figure 2 Preliminary results to select CNPW concentration. A) Trend of dead cell percentage quantified by flow cytometry of hSDFs untreated and after CNPW treatments. B) Flow cytometry of hSDFs exposed to increasing concentration of CNPW (range 10-100 mg/mL), evaluating forward scatter (FSC) and side scatter (SSC). C) Median SSC values (±standard deviation) of three independent experiments.

Figure 3 Sub-confluent hSDFs are incubated with 50 mg/L CNPW alone or in combination with B(α)P 20 µg /L for 24 h (Panels A, B, C) or after 8 days (Panels D, E, F); hSDFs untreated (Panels A, D), treated with CNPW (Panels B, E) or with CNPW+B(α)P (Panels C, F) are stained with Mitotracker, as described in the Materials and Methods. Using a confocal microscope are acquired in reflection mode the aggregates of nanoparticles. Yellow brackets show the CNPW aggregates in the cytoplasm of the cell.

Figure 4 Changes (% volume/volume) of protein regulation in fibroblasts hSDF exposed to B(α)P 20 µg/L (A), CNPW 50 mg/L (B) and CNPW 50 mg/L-B(α)P complex 20 µg/L (C). Down-regulation is indicated in green, while up-regulation is shown in blue (Student t-test, *p<0,05, **p<0,01).
HSPA8=Heat shock cognate 71 kDa protein; UBA52=Ubiquitin-60S ribosomal protein L40; HSPB1=Heat shock protein beta-1; VIM=Vimentin; HSPB1=Heat shock protein beta-1; CLIC4=Chloride intracellular channel protein 4; ANXA2=Annexin A2; TPI1=Triosephosphate isomerase; ENO1=α-enolase; APRT=Adenine phosphoribosyl-transferase; CFL1=Cofilin-1; GAPDH=Glyceraldehyde-3-phosphate dehydrogenase; ALDOA=Fructose-bisphosphate aldolase A; PRDX2=Peroxiredoxin-2; NME1=Nucleoside diphosphate kinase A; GSTP1=Glutathione S-transferase P; PGK1=Phosphoglycerate kinase 1; PFN1=Profilin-1; PPIA=Peptidyl-prolyl cis-trans isomerase A; PKM=Pyruvate kinase PKM; ARHGDIA=Rho GDP-dissociation inhibitor 1; HSPD1=60 kDa Heat shock protein, mitochondrial; TKT=Transketolase; PSME2=Proteasome activator complex subunit 2.

Figure 5 The four metabolic networks in which many identified proteins are involved. A) glycolysis and pentose phosphate pathway; B) cytoskeleton formation and apoptosis; C) stress response; D) vesicle transport control.

Figure 6 Diagram of the correlation between glycolysis and pentose phosphate pathway (PPP). Proteins changed by the complex CNPW+B(α)P are indicated in red squares (blue arrows=down-regulation; green arrows=up-regulation).
PGLS=6-phosphogluconolactonase; PGD=6-phosphogluconate dehydrogenase; RPI=ribose-5-phosphate isomerase; TKT=transketolase; T-ALDO=transaldolase; G6PD=glucose-6-phosphate 1-dehydrogenase; HK=hexokinase; PGI=glucose-6-phosphate isomerase; PFK=phosphofructokinase; ALDOA= fructose-bisphosphate aldolase A; GAPDH=glyceraldehyde-3-phosphate dehydrogenase; TPI1=triosephosphate isomerase; PGK1=phosphoglycerate kinase 1; PGM=phosphoglycerate mutase; ENO1=α-enolase; PKM=pyruvate kinase.

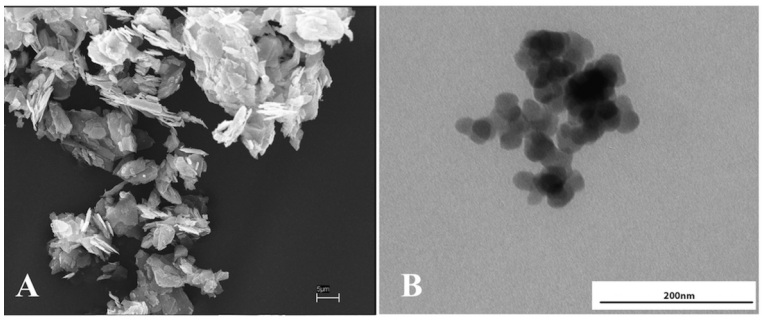
A
5μm
B
200nm

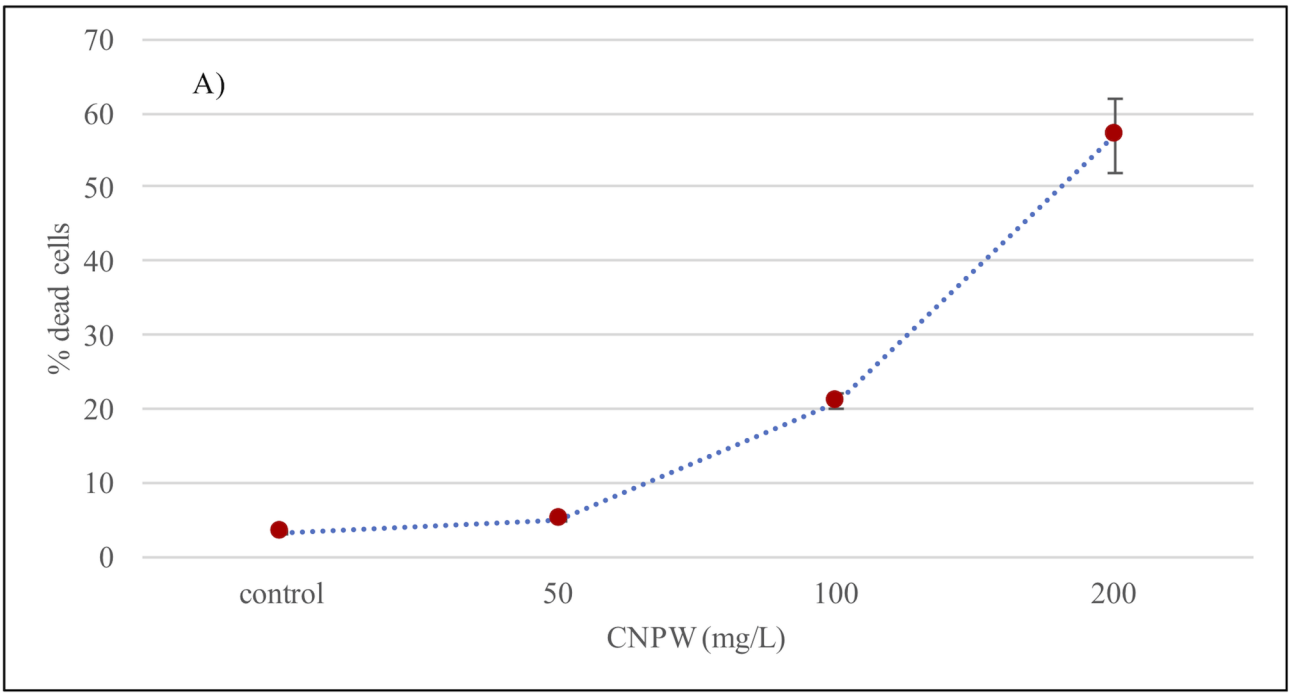

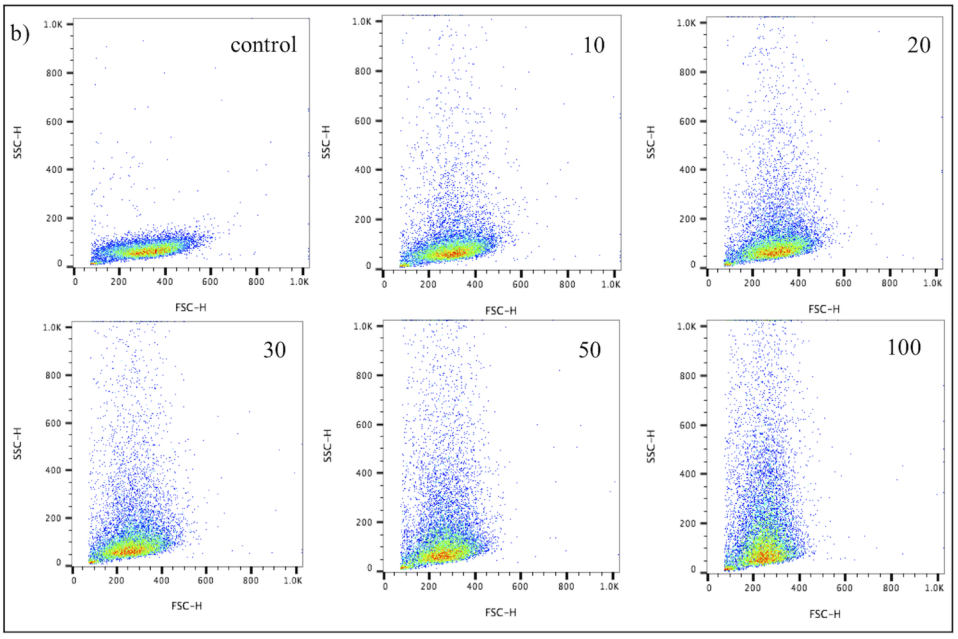

c)

CNPW mg/L	SSC
control	68±15
10	76±20
20	82±18
30	86±16
50	95±25
100	120±30

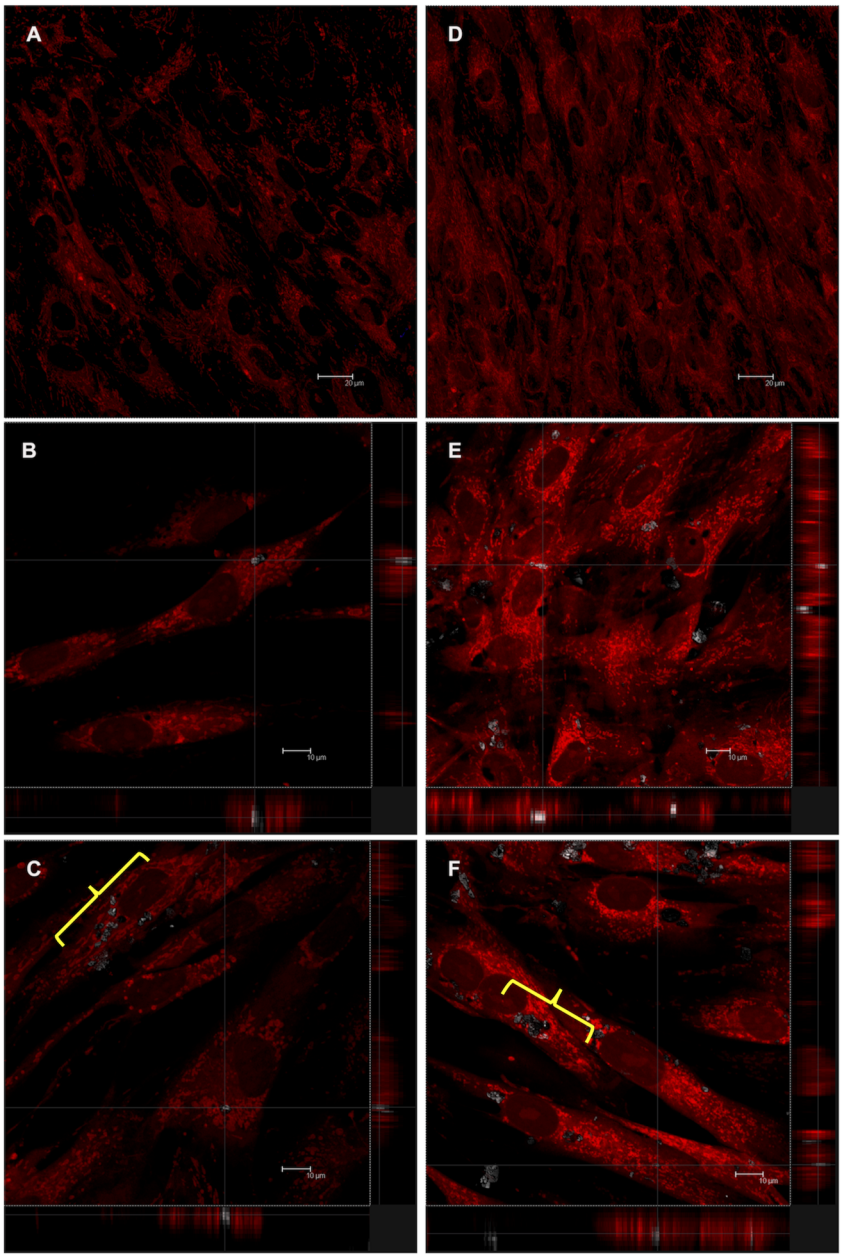
A
D
B
E
C
F

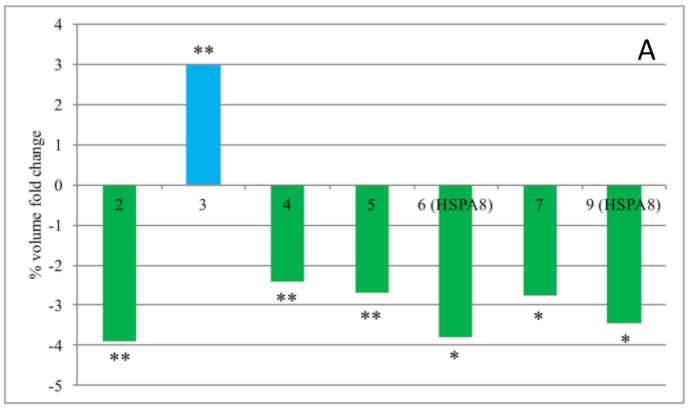
A
% volume fold change
4
3
2
1
0
-1
-2
-3
-4
-5
2
3
4
5
6 (HSPA8)
7
9 (HSPA8)

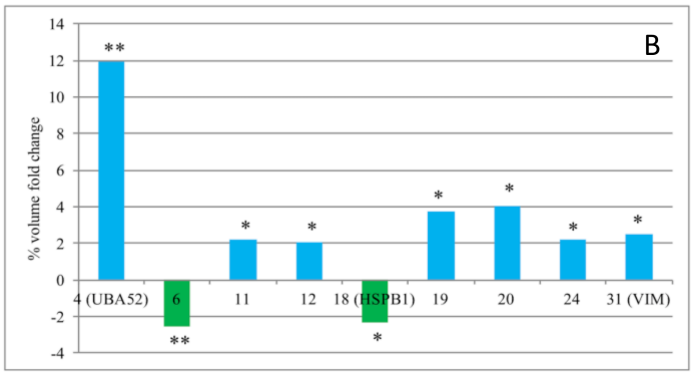
B
% volume fold change
14
12
10
8
6
4
2
0
-2
-4
4 (UBA52)
6
11
12
18 (HSPB1)
19
20
24
31 (VIM)

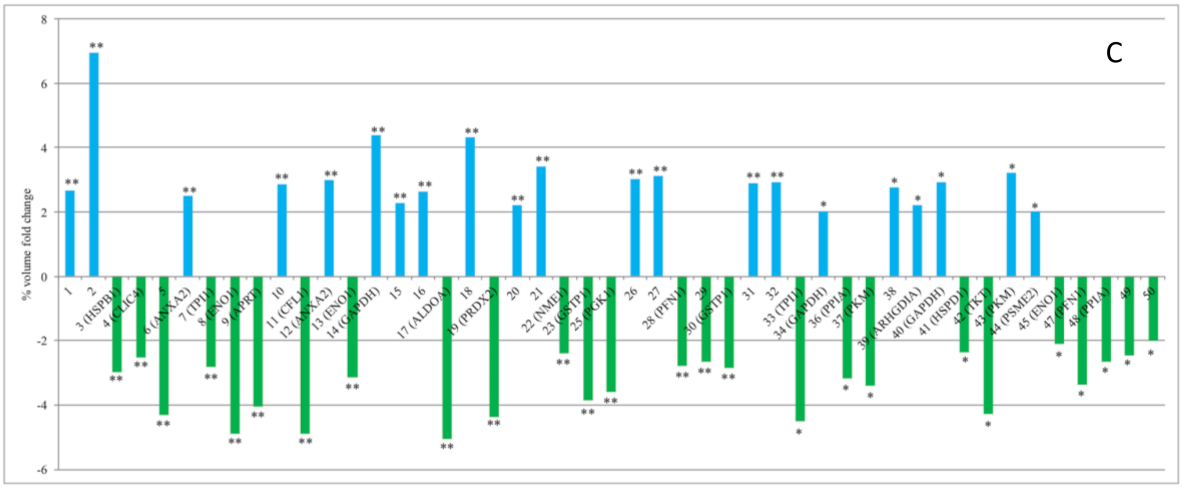
C
% volume fold change
8
6
4
2
0
-2
-4
-6

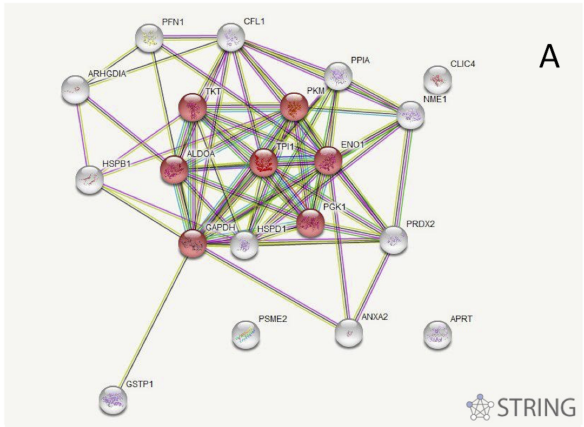
A
PFN1
CFL1
PPIA
CLIC4
ARHGDIA
TKT
PKM
NME1
TPI1
ENO1
ALDOA
HSPB1
PGK1
GAPDH
HSPD1
PRDX2
PSME2
ANXA2
APRT
GSTP1
STRING

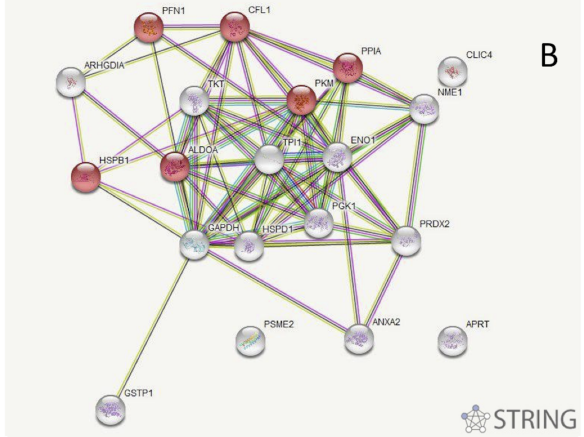
B
PFN1
CFL1
PPIA
CLIC4
ARHGDIA
TKT
PKM
NME1
TPI1
ENO1
ALDOA
HSPB1
PGK1
GAPDH
HSPD1
PRDX2
PSME2
ANXA2
APRT
GSTP1
STRING

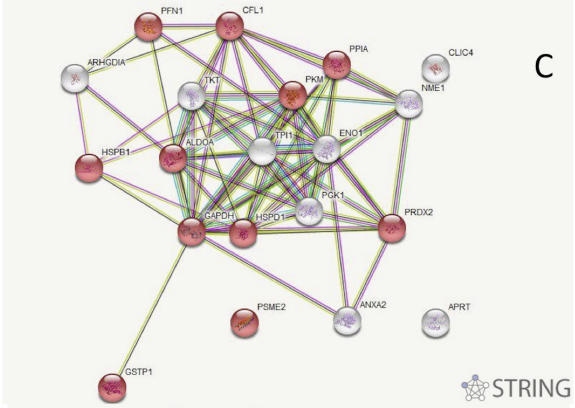
C
PFN1
CFL1
PPIA
CLIC4
ARHGDIA
TKT
PKM
NME1
TPI1
ENO1
ALDOA
HSPB1
PGK1
GAPDH
HSPD1
PRDX2
PSME2
ANXA2
APRT
GSTP1
STRING

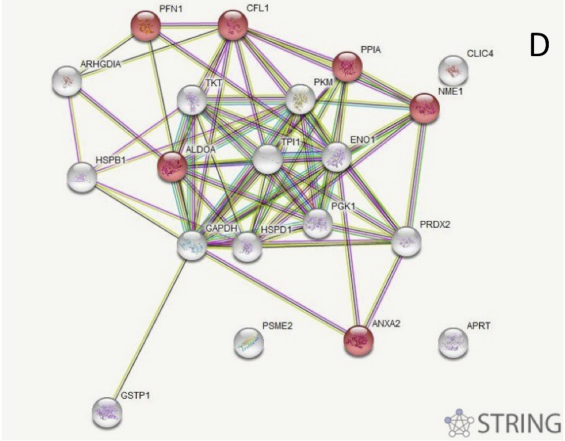
D
PFN1
CFL1
PPIA
CLIC4
ARHGDIA
TKT
PKM
NME1
TPI1
ENO1
ALDOA
HSPB1
PGK1
GAPDH
HSPD1
PRDX2
PSME2
ANXA2
APRT
GSTP1
STRING

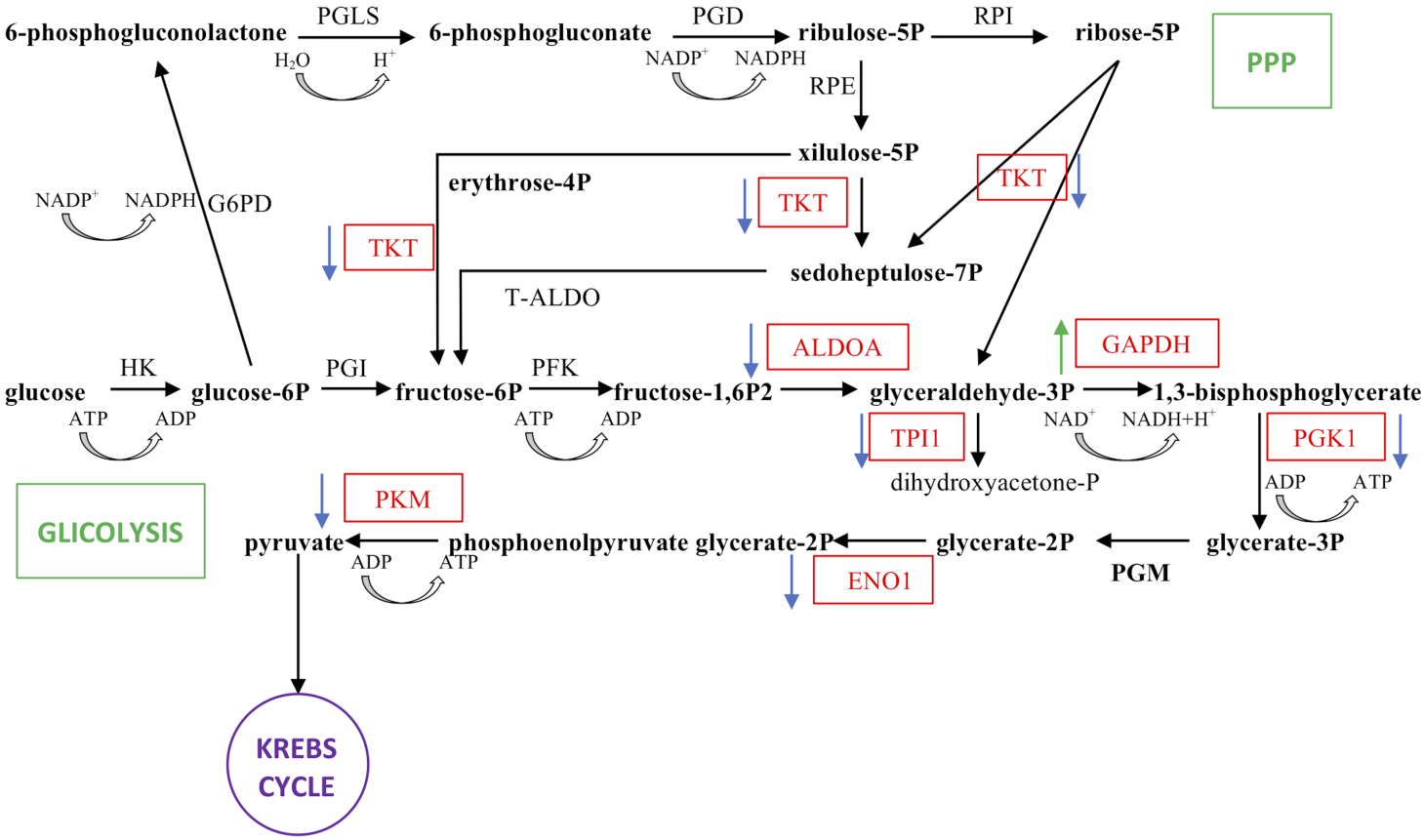
6-phosphogluconolactone
PGLS
H2O
H+
6-phosphogluconate
PGD
NADP+
NADPH
ribulose-5P
RPI
ribose-5P
PPP
RPE
xilulose-5P
TKT
erythrose-4P
TKT
NADP+
NADPH
G6PD
TKT
sedoheptulose-7P
T-ALDO
ALDOA
GAPDH
glucose
HK
ATP
ADP
glucose-6P
PGI
fructose-6P
PFK
ATP
ADP
fructose-1,6P2
glyceraldehyde-3P
NAD+
NADH+H+
1,3-bisphosphoglycerate
TPI1
dihydroxyacetone-P
PGK1
ADP
ATP
GLICOLYSIS
PKM
pyruvate
ADP
ATP
phosphoenolpyruvate
glycerate-2P
ENO1
glycerate-2P
PGM
glycerate-3P
KREBS CYCLE

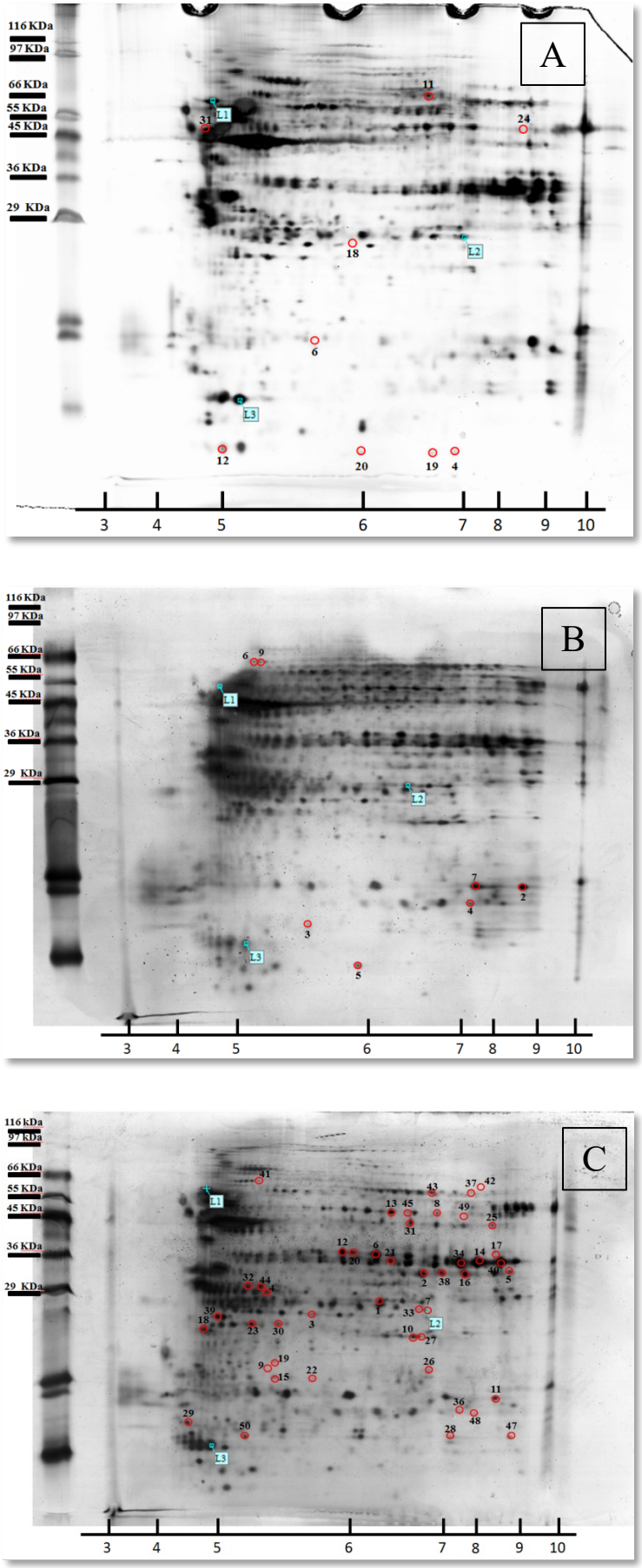

Figure S1 Protein pattern of hSDF exposed to CNPW 50 mg/L (A), B(α)P 20 µg/L (B) and CNPW 50 mg/L+B(α)P 20 µg/L (C). Spots significantly ($p<0.05$) different (volume/volume) to controls are shown in red.